Carcinogenesis vol.30 no.8 pp.1320–1329, 2009
doi:10.1093/carcin/bgp138
Advance Access publication June 5, 2009

Triggering of transient receptor potential vanilloid type 1 (TRPV1) by capsaicin induces Fas/CD95-mediated apoptosis of urothelial cancer cells in an ATM-dependent manner

Consuelo Amantini[1,*], Patrizia Ballarini[2], Sara Caprodossi[1], Massimo Nabissi[1], Maria Beatrice Morelli[1,3], Roberta Lucciarini[1], Marco Andrea Cardarelli[4], Gabriele Mammana[5] and Giorgio Santoni[1]

[1]Department of Experimental Medicine and Public Health and [2]Department of Molecular, Cellular and Animal Biology, University of Camerino, via Madonna delle Carceri 9, 62032 Camerino (MC), Italy, [3]Department of Experimental Medicine, University ''La Sapienza'', 00161 Rome, Italy, [4]Pathology and Cytodiagnostic Unit and [5]Urology Operative Unit, ASUR 9, 62100 Macerata, Italy

[*]To whom correspondence should be addressed. Tel: +39 0737 403319; Fax: +39 0737 403325;
Email: giorgio.santoni@unicam.it

Herein, we provide evidence on the expression of transient receptor potential vanilloid type 1 (TRPV1) on human urothelial cancer (UC) cells and its involvement in the apoptosis induced by the selective agonist capsaicin (CPS). We analyzed TRPV1 messenger RNA and protein expression on human UC cell lines demonstrating its progressive decrease in high-grade UC cells. Treatment of RT4 cells with CPS induced cell cycle arrest in G_0/G_1 phase and apoptosis. These events were associated with rapid co-ordinated transcription of pro-apoptotic genes including Fas/CD95, Bcl-2 and caspase families and ataxia telangiectasia mutated (ATM)/CHK2/p53 DNA damage response pathway. CPS induced Fas/CD95 upregulation, but more importantly Fas/CD95 ligand independent, TRPV1-dependent death receptor clustering and triggering of both extrinsic and intrinsic mitochondrial-dependent pathways. Moreover, we observed that CPS activates ATM kinase that is involved in Ser15, Ser20 and Ser392 p53 phosphorylation as shown by the use of the specific inhibitor KU55933. Notably, ATM activation was also found to control upregulation of Fas/CD95 expression and its co-clustering with TRPV1 as well as RT4 cell growth and apoptosis. Altogether, we describe a novel connection between ATM DNA damage response pathway and Fas/CD95-mediated intrinsic and extrinsic apoptotic pathways triggered by TRPV1 stimulation on UC cells.

Introduction

Capsaicin (CPS), a homovanillic acid derivate, is an active component of the red pepper, genus *Capsicum*, shown to inhibit the growth of a number of tumor cells by inducing apoptosis (1–3). Most of CPS pro-apoptotic effects are mediated by the transient receptor potential vanilloid type 1 (TRPV1), a non-selective cation channel belonging to the TRP family of ion channels (3–5), and have been recently associated with endoplasmic reticulum (ER) stress (6,7).

TRPV1 is expressed predominantly on nociceptive neurons, but it has been recently found also in non-neuronal cells (8). In this regard, in the urinary bladder, TRPV1 is expressed both in the afferent sensory neurons and on basal and apical urothelial cells (9). Pain perception was the first role attributed to TRPV1 in the urinary tract; moreover, urothelial TRPV1 has been described to sense mechanical and irritant stimuli (10,11).

Recent evidence also suggests that TRPV1 contributes to growth and progression of several malignancies (3,12,13). In this regard, a progressive loss of TRPV1 expression on transitional cell carcinomas of human urinary bladder was recently reported (14), but its functional relevance in urothelial cancer (UC) is still unknown.

In accordance with the previous data (15), we have recently shown that CPS results in a TRPV1-dependent mitochondrial-mediated apoptosis of glioma cells through the activation of p38 mitogen-activated protein kinase (3); however, TRPV1 activation can also inhibit cancer cell growth via non-apoptotic mechanisms (16).

Herein, we demonstrate that TRPVI messenger RNA (mRNA) and protein expression was strongly down-modulated in high grade as compared with low-grade superficial UC cells. Moreover, we provide the first evidence that CPS-induced TRPV1-mediated apoptosis of UC cells not only involves the mitochondrial pathway but also is associated with CPS-induced TRPV1-Fas/CD95 co-clustering and activation of the extrinsic apoptotic pathway. Finally, consistent with the ability of CPS to act as ER stressor, we found that CPS-induced TRPVI-mediated apoptosis is dependent on ataxia telangiectasia mutated (ATM)-mediated p53 activation.

Abbreviations: Ab, antibody; ATM, ataxia telangiectasia mutated; CPS, capsaicin; CPZ, capsazepine; ER, endoplasmic reticulum; FACS, fluorescent activated cell sorting; FITC, fluorescein isothiocyanate; GAM, goat anti-mouse; HRP, horseradish peroxidase; JC-1, 5,5′,6,6′-tetrachloro-1,1′,3,3′-tetraethylbenzimidazolcarbocyanine iodide; mAb, monoclonal antibody; mRNA, messenger RNA; MTT, 3-(4,5-dimethylthiazol-2-yl)-2,5-diphenyltetrazolium bromide; NHUC, normal human urothelial cells; PBS, phosphate-buffered saline; PCR, polymerase chain reaction; RAG, rabbit anti-goat; RT, reverse transcription; SDS–PAGE, sodium dodecyl sulfate–polyacrylamide gel electrophoresis; TRPV1, transient receptor potential vanilloid type 1; UC, urothelial cancer.

Materials and methods

UC cell lines

Normal human urothelial cells (NHUC) from Oligene (Berlin, Germany) were cultured in Oligene Urothelial Cell Media System. Human well-differentiated low-grade papillary RT4 and poorly differentiated, high-grade and muscle invasive UC J82, EJ and TCCSUP cell lines were from American Type Culture Collection (Rockville, MD) and were maintained in RPMI-1640 medium (Flow Laboratories, Irvine, UK) supplemented with 10% heat-inactivated fetal calf serum (Euroclone Ltd, Devon, UK), *N*-2-hydroxyethylpiperazine *N*′-2-ethanesulfonic acid, 2mM L-glutamine, 100 IU/ml of penicillin and 100 μg/ml of streptomycin at 37°C, 5% CO_2 and 95% of humidity.

Antibodies and reagents

The following antibodies (Abs) were used: goat anti-human TRPV1 from Santa Cruz Biotechnology (Santa Cruz, CA); rabbit anti-human p53, rabbit anti-human phospho-p53 (Ser20), rabbit anti-human phospho-p53 (Ser392) and rabbit anti-human BID from Cell Signaling (Danvers, MA); rabbit anti-human caspase-3 and caspase-9 from Calbiochem–Novabiochem Corporation (San Diego, CA) and rabbit anti-human phosphoATM (Ser1981) from RD Systems (South Beloit, IL). The following monoclonal antibodies (mAbs) were used: anti-human phospho-p53 (Ser15) from Santa Cruz Biotechnology; anti-human caspase-8 from BD Biosciences (San Josè, CA); anti-human α-tubulin from Millipore (Billerica, MA); anti-human caspase-9 from Millipore and anti-human Fas and anti-human GAPDH from Sigma–Aldrich (St Louis, MO).

The horseradish peroxidase (HRP)-conjugated donkey anti-goat from Santa Cruz Biotechnology; the HRP-conjugated sheep anti-mouse and the HRP-conjugated donkey anti-rabbit polyclonal Abs from GE-Healthcare (Piscataway, NJ). Purified fluorescein isothiocyanate (FITC)-conjugated rabbit anti-goat (RAG) IgG (EMD Chemicals, San Diego, CA), goat anti-mouse (GAM) Alexa Fluor 594, RAG Alexa Fluor 488 (Invitrogen, San Diego, CA) and phycoerythrin-conjugated GAM (EMD Chemicals) were used as secondary Abs control.

CPS ([*N*-(4-hydroxy-3-methoxy-phenyl)methyl]-8-methyl-6-nonenamide), capsazepine (CPZ) (*N*-[2-(4-chlorophenyl)ethyl]-1,3,4,5-tetrahydro-7,8-dihydroxy-2H-2-benzazepine-2-carbothioamide), 3-(4,5-dimethylthiazol-2-yl)-2,5-diphenyltetrazolium bromide (MTT), dimethyl sulfoxide, the ATM-specific inhibitor KU55933 and carbonyl cyanide chlorophenylhydrazone were obtained from Sigma–Aldrich; SB366791 (4′-chloro-3-methoxycinnamanilide) was purchased from Tocris Bioscience (Bristol, UK). FITC-conjugated annexin V was purchased from Axxora LLC (San Diego, CA). Propidium iodide and 5,5′,6,6′-tetrachloro-1,1′,3,3′-tetraethylbenzimidazolcarbocyanine iodide (JC-1) were obtained from Invitrogen; the caspase-8 inhibitor Z-IETD-FM (KZ-Ile-Glu(O-ME)-Thr-Asp(O-Me) fluoromethyl ketone) was from

Sigma–Aldrich. CPS, CPZ and KU55933 stock solutions were dissolved in dimethyl sulfoxide.

RNA isolation and reverse transcription

Total RNA was extracted from NHUC, used as control, and from RT4, TCCSUP, J82 and EJ cells using RNeasy Mini kit (Qiagen, Milan, Italy). In brief, cultured cells were first collected by centrifugation for 5 min at 5000*g*, washed in phosphate-buffered saline (PBS) for 5 min at 5000*g* and then processed for total RNA extraction.

All RNA samples were dissolved in RNAse-free water (Sigma–Aldrich) and their concentration and purity were evaluated by A_{260nm} measurement. Two micrograms of RNA extracted from each sample was subjected to reverse transcription (RT) in a total volume of 50 µl using the High-Capacity cDNA Archive Kit (PE Applied Biosystems, Foster City, CA). The RT mixtures were incubated for 10 min at 25°C and for 2 h at 37°C. In all samples, 2 µl of the resulting complementary DNA products were used as template for polymerase chain reaction (PCR) quantification.

Quantitative real-time PCR

Quantitative real-time PCR was performed using an IQ5 Multicolor Real-time PCR Detection system (Bio-Rad, Hercules, CA) and the reaction mixture contained the Taqman Universal PCR Master Mix and primer and probe sets (Applied Biosystems, Foster City, CA). Human TRPV1 primers and probe were purchased as 'assay on demand' (cod. Hs00218912_m1) by Applied Biosystems. β-Actin primers and probe sequence (forward—5′-CTGGAACGGTGAAGGTGACA-3′ and reverse—5′-CGGCCACATTGTGAACTTTG-3′; probe—5′-CAGTCGGTTGGAGCGAGCATCCC-3′) were designed by Primer Express Software (PE Applied Biosystems) and purchased from Sigma Genosys (St. Louis, MO). Each PCR amplification consisted of heat activation for 2 min at 50°C and for 10 min at 95°C followed by 40 cycles of 95°C for 10 s and 60°C for 1 min. All samples were assayed in triplicate in the same plate. Measurement of β-actin levels on the UC cell lines was used to normalize mRNA contents, and TRPV1 levels were expressed as relative fold compared with the corresponding control calculated by the $2^{-\Delta\Delta Ct}$ method.

Immunofluorescence and flow cytometry

To determine the expression of TRPV1, 3×10^5 UC cells were fixed and permeabilized using CytoFix/CytoPerm Plus (BD Biosciences, Milano, Italy) before the addition of anti-TRPV1 Ab directed against a peptide mapping near the C-terminus of human protein (1:25 dilution). Normal goat serum was used as negative control. After 30 min at 4°C, cells were washed twice with PBS without calcium and magnesium (Euroclone Ltd) and then labeled with FITC-conjugated RAG (1:40 dilution). The percentage of positive cells determined over 10 000 events was analyzed on an FACScan cytofluorimeter (Becton Dickinson, Franklin Lakes, NJ) and fluorescent intensity is expressed in arbitrary units on a logarithmic scale. Moreover, RT4 cells, untreated or treated with CPS (100 µM) alone or in combination with the ATM inhibitor KU55933 (10 µM) for different times (8, 12 and 24 h), were stained with anti-Fas/CD95 (1:25) mAb followed by phycoerythrin-conjugated GAM (1:40) secondary Ab.

Confocal laser scanning microscopy analysis

A total of 2×10^5/ml cells from UC cell lines grown for 24 h at 37°C and 5% CO_2 in poly-L-lysine-coated slides were permeabilized using 2% of paraformaldehyde with 0.5% of Triton X-100 in PBS and fixed by 4% of paraformaldehyde in PBS. After three washes in PBS, cells were incubated with 3% of bovine serum albumin and 0.1% of Tween-20 in PBS for 1 h at room temperature and then with a goat anti-TRPV1 (1:25) Ab overnight at 4°C. Samples were finally washed with 0.3% of Triton X-100 in PBS three times, incubated with RAG Alexa Fluor 488 (1:100) for 1 h at 37°C, mounted and analyzed with MRC600 confocal laser scanning microscope (BioRad) equipped with a Nikon (Diaphot-TMD) inverted microscope.

In some experiments, untreated or CPS (100 µM)-treated RT4 cells for different times (0, 4, 8, 12 and 24 h) were incubated with anti-human Fas/CD95 mAb (1:25) followed by GAM Alexa Fluor 594 (1:100). In order to evaluate the colocalization of Fas/CD95 with TRPV1, RT4 cells, treated for 24 h with CPS (100 µM) alone or in combination with CPZ (10 µM), were incubated with both anti-human Fas mAb and goat anti-human TRPV1 Ab followed by the respective secondary Abs. The role of ATM was evaluated by treatment of RT4 cells for 24 h with CPS in combination with KU55933 inhibitor (10 µM). Colocalization of Fas/CD95 with TRPV1 was analyzed as above described. Fluorochrome was excited with the 600 line of an argon–krypton laser and imaged using a 488 (FITC) nm bandpass filter. Serial optical sections were taken at 1 µm intervals through the cells. Images were processed using Jacs Paint Shop Pro (Jacs Teckraft Sotfware Pvt. Ltd., Chennai, India).

Western blot analysis

Lysates obtained from NHUC, used as control, RT4, TCCSUP, J82 and EJ cells were resuspended in 0.2 ml of lysis buffer [10 mM Tris, pH 7.4; 100 mM NaCl; 1 mM ethylenediaminetetraacetic acid; 1 mM ethyleneglycol-bis(aminoethylether)-tetraacetic acid; 1 mM NaF; 20 mM $Na_4P_2O_7$; 2 mM Na_3VO_4; 1% Triton X-100; 10% glycerol; 0.1% sodium dodecyl sulfate; 0.5% deoxycholate and 1 mM phenylmethylsulfonyl fluoride and protease inhibitor cocktail from Sigma].

Samples were separated on 7.5% sodium dodecyl sulfate–polyacrylamide gel electrophoresis (SDS–PAGE), transferred onto Immobilon-P membranes (Millipore, Bedford, MA) and blotted with anti-TRPV1 Ab (1:400) followed by the incubation with HRP-conjugated donkey anti-goat (1:200).

In some experiments, lysates from untreated or CPS (100 µM)-treated RT4 cells for different times (0, 10, 30, 60 and 180 min) were separated on 6% SDS–PAGE and immunoblotted with a rabbit anti-phospho ATM Ab (1 µg/ml) followed by HRP-conjugated donkey anti-rabbit Ab (1:10000).

In addition, lysates from RT4 cells, treated for different times (1, 3, 6, 12 and 24 h) with CPS (100 µM) alone or in combination with KU55933 (10 µM), were separated on 9% SDS–PAGE and immunoblotted with anti-p53 (1:1000), anti-phospho-p53 (Ser20) (1:1000) and anti-phospho-p53 (ser392) (1:1000) Abs, followed by the incubation with HRP-conjugated donkey anti-rabbit (1:10000) Ab or with an anti-phospho-p53 (Ser15) mAb (1:2000) followed by HRP-conjugated sheep anti-mouse Ab (1:10000). Furthermore, lysates from RT4 cells treated for different times with CPS were separated on 12% and on 14% SDS–PAGE and immunoblotted with anti-caspase-8 mAb, anti-caspase-9 mAb, rabbit polyclonal anti-BID or anti-caspase-3 Ab, respectively, followed by HRP-conjugated secondary Abs. Anti-α-tubulin and anti-GAPDH mAbs were used as protein loading control.

In addition, to evaluate cytochrome c release, untreated or CPS-treated RT4 cells at different times (8, 12 and 24 h) were washed in ice-cold PBS and the resulting pellet was resuspended in 0.2 ml of lysis buffer (20 mM *N*-2-hydroxyethylpiperazine *N*′-2-ethanesulfonic acid, 10 mM KCl, 1.5 mM $MgCl_2$, 1 mM ethylenediaminetetraacetic acid, 1 mM ethyleneglycol-bis(aminoethylether)-tetraacetic acid, 1 mM dithiothreitol and 0.1 mM phenylmethylsulfonyl fluoride) supplemented with protease inhibitors (5 µg/ml pepstatin A, 10 µg/ml leupeptin and 2 µg/ml aprotinin). After sitting on ice for 15 min, cells were disrupted by 60 times douncing in a mini-potter. The nuclei were pelletted at 1000*g* for 5 min at 4°C and the supernatants were separated and centrifuged for 40 min at 80 000*g*. Then, supernatants loaded onto a 14% SDS–PAGE were transferred overnight at 20 V and incubated with anti-cytochrome c mAb (0.5 µg/ml) for 2 h, followed by HRP-conjugated anti-mouse (1:10000) Ab. Immunoreactivity was detected using the Enhanced Chemiluminescence (Amersham, Piscataway, NJ). Densitometric analysis was performed by a Chemidoc using the Quantity One software (Bio-Rad). Each sample was compared with its control (α-tubulin) for the purpose of quantification.

MTT assay

The colorimetric MTT assay that measures the mitochondrial conversion of the tetrazolium salt to a blue formizan salt was used to evaluate the growth of CPS-treated UC cell lines. Briefly, 8×10^4 UC cells were treated for 24 h at 37°C and 95% of humidity with different doses of CPS (10–100 µM). In some experiments, RT4 cells were treated with CPS in combination with CPZ (10 µM) or with SB366791 (0.1 µM) or with KU55933 (10 µM) in a 96-well microtiter plates and incubated for the last 3 h with 20 µl per well of MTT (5 mg/ml). Then supernatants were discarded and colored formazan crystals, dissolved with 100 µl per well of dimethyl sulfoxide and were read by an enzyme-linked immunosorbent assay reader (BioTek Instruments, Winooski, VT).

Cell cycle analysis

A total of 3×10^5/ml RT4 cells were grown with CPS (100 µM) alone or in combination with CPZ (10 µM) or with SB366791 (0.1 µM), for 24 h at 37°C and 5% CO_2. After washing in PBS, cells were fixed for 30 min on ice by adding 1 ml of 70% cold ethanol, centrifuged in order to discard ethanol, stained for 15 min at room temperature with PI 20 µg/ml in DNAse-free PBS and finally analyzed by flow cytometry. The percentage of positive cells determined over 10 000 events was analyzed on an FACScan cytofluorimeter using the Cell Quest software (Becton Dickinson). Fluorescent intensity is expressed in arbitrary units on a logarithmic scale.

Annexin V staining

Phosphatidylserine exposure on RT4 cells was detected by annexin V staining and cytofluorimetric analysis. Briefly, 2×10^5/ml RT4 cells were treated with CPS (100 µM) or with vehicle, for different times (6, 12 and 24 h) at 37°C, 5% CO_2, in a 24-well plate. After treatment, cells were stained with annexin V-FITC for 10 min at room temperature, then detached by scraping and washed once with binding buffer (10 mM *N*-2-hydroxyethylpiperazine *N*′-2-ethanesulfonic acid/NaOH, pH 7.4; 140 mM NaCl and 2.5 mM $CaCl_2$). Samples were analyzed by an FACScan cytofluorimeter using the Cell Quest software. In some experiments, cells were treated for 24 h with CPS (100 µM) in combination with CPZ (10 µM) or with SB366791 (0.1 µM) or with KU55933 (10 µM).

RT profiler PCR array

Total RNA from RT4 cells, untreated or treated for 4 and 12 h with CPS (100 μM), was isolated as above described. Two micrograms of RNA extracted from each sample was subjected to RT in a total volume of 20 μl using the ReactionReady™ first strand cDNA (Superarray Bioscience Corporation, Frederick, MD). RT mixtures were incubated for 60 min at 37°C, 5 min at 95°C and stored at −20°C until the next step.

Quantitative RT–PCR was performed using an IQ5 Multicolor Real-time PCR Detection system (BioRad), the SuperArray's RT^2 real-time SYBR Green PCR Master Mix and the Human Pathways CancerFinder™ and Human apoptosis plates (Superarray Bioscience Corporation). Each PCR amplification consisted of heat activation for 10 min at 95°C followed by 40 cycles of 95°C for 15 s and 60°C for 1 min. Measurement of five housekeeping genes levels on the samples was used to normalize mRNA content and the expression levels of 168 different genes were expressed as relative fold of the corresponding control according to the protocol (Superarray Bioscience Corporation).

Mitochondrial transmembrane potential $\Delta\psi_m$

$\Delta\psi_m$ was evaluated by JC-1 staining. Briefly, 2×10^5 RT4 cells/ml resuspended in RPMI/fetal calf serum treated with 100 μM of CPS alone or in combination with caspase-8 inhibitor Z-IETD-FM, for different times (8, 12 and 24 h) at 37°C in 5% CO_2, were incubated for 10 min at room temperature with 300 μl of 10 μg/ml JC-1 and analyzed by an FACscan cytofluorimeter (Becton Dickinson). JC-1 was excited by an argon laser (488 nm) and green (530 nm)/red (>570 nm) emission fluorescence was collected simultaneously. Data were analyzed using the Cell Quest software. Carbonyl cyanide chlorophenylhydrazone protonophore, a mitochondrial uncoupler that collapses $\Delta\psi_m$, was used as positive control (data not shown).

Statistical analysis

The statistical significance was determined by Student's *t*-test and by Bonferroni test (analysis of variance one way).

Results

TRPV1 mRNA and protein expression on UC cell lines

We first determined the expression of TRPV1 both at mRNA and protein levels in low-grade RT4 and high-grade TCCSUP, J82 and EJ UC cell lines and in NHUC used as control. Quantitative RT–PCR showed high levels of TRPV1 mRNA in RT4 cells that were

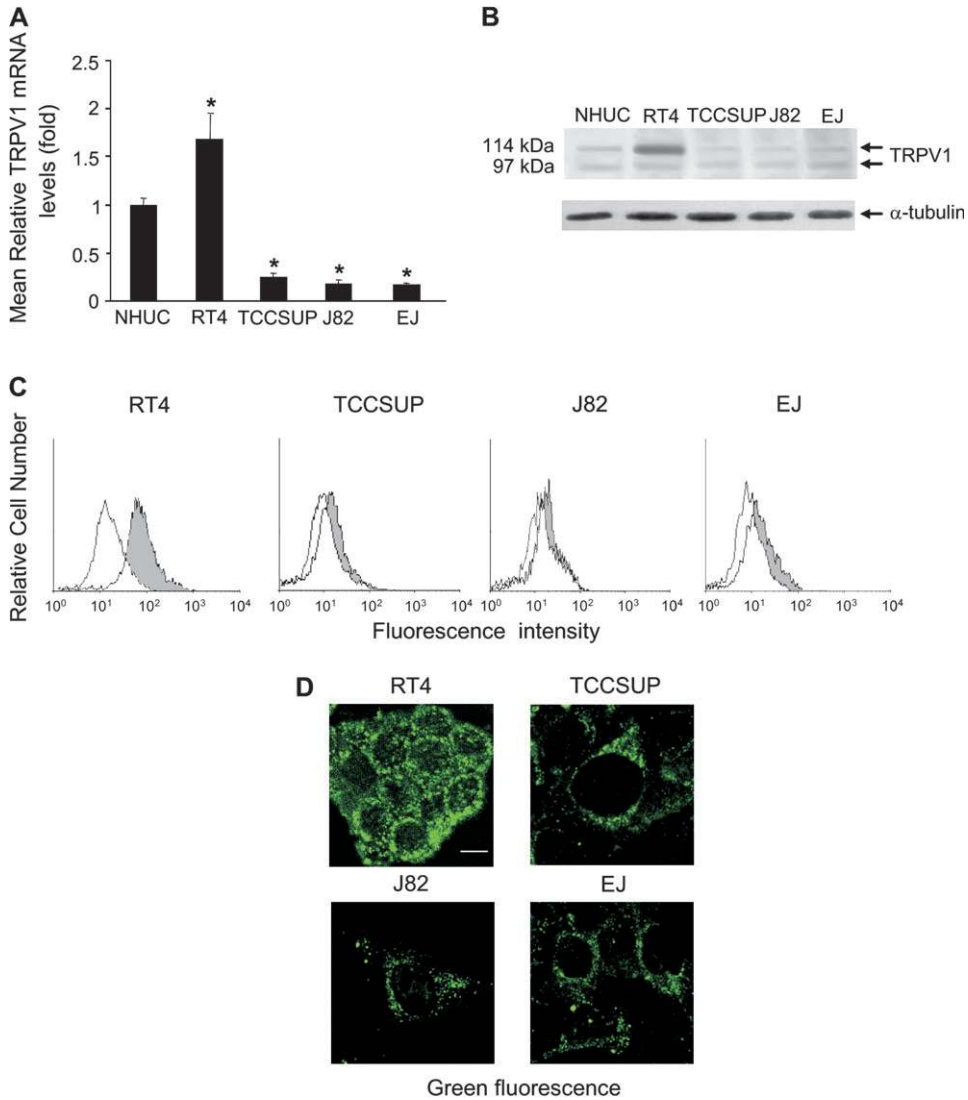

Fig. 1. TRPV1 mRNA and protein expression in UC cell lines. (**A**) TRPV1 mRNA levels from RT4, TCCSUP, J82 and EJ UC cell lines were evaluated by quantitative RT–PCR. TRPV1 mRNA levels (mean ± SD) were expressed as relative fold with respect to NHUC used as control. Values were normalized for β-actin expression. Statistical analysis was performed comparing RT4, TCCSUP, J82 and EJ cell lines with control; $^*P < 0.01$. (**B**) Lysates from NHUC or the indicated UC cell lines were separated on 7.5% SDS–PAGE and probed with a goat anti-human TRPV1 Ab or anti-human α-tubulin mAb. Arrows indicate the bands corresponding to TRPV1 and α-tubulin proteins. Sizes are shown in kilodaltons (kDa). Data are representative of three separate experiments. (**C**) TRPV1 expression in UC cell lines was evaluated by immunofluorescence and FACS analysis using a goat anti-human TRPV1 Ab. FITC-conjugated RAG was used as secondary Ab. White area indicates secondary Ab alone used as negative control. (**D**) Immunocytochemical TRPV1 localization in UC cell lines was evaluated by confocal microscopy. Goat anti-human TRPV1 Ab and FITC-conjugated RAG were used as primary and secondary Abs, respectively; bar = 10 μm.

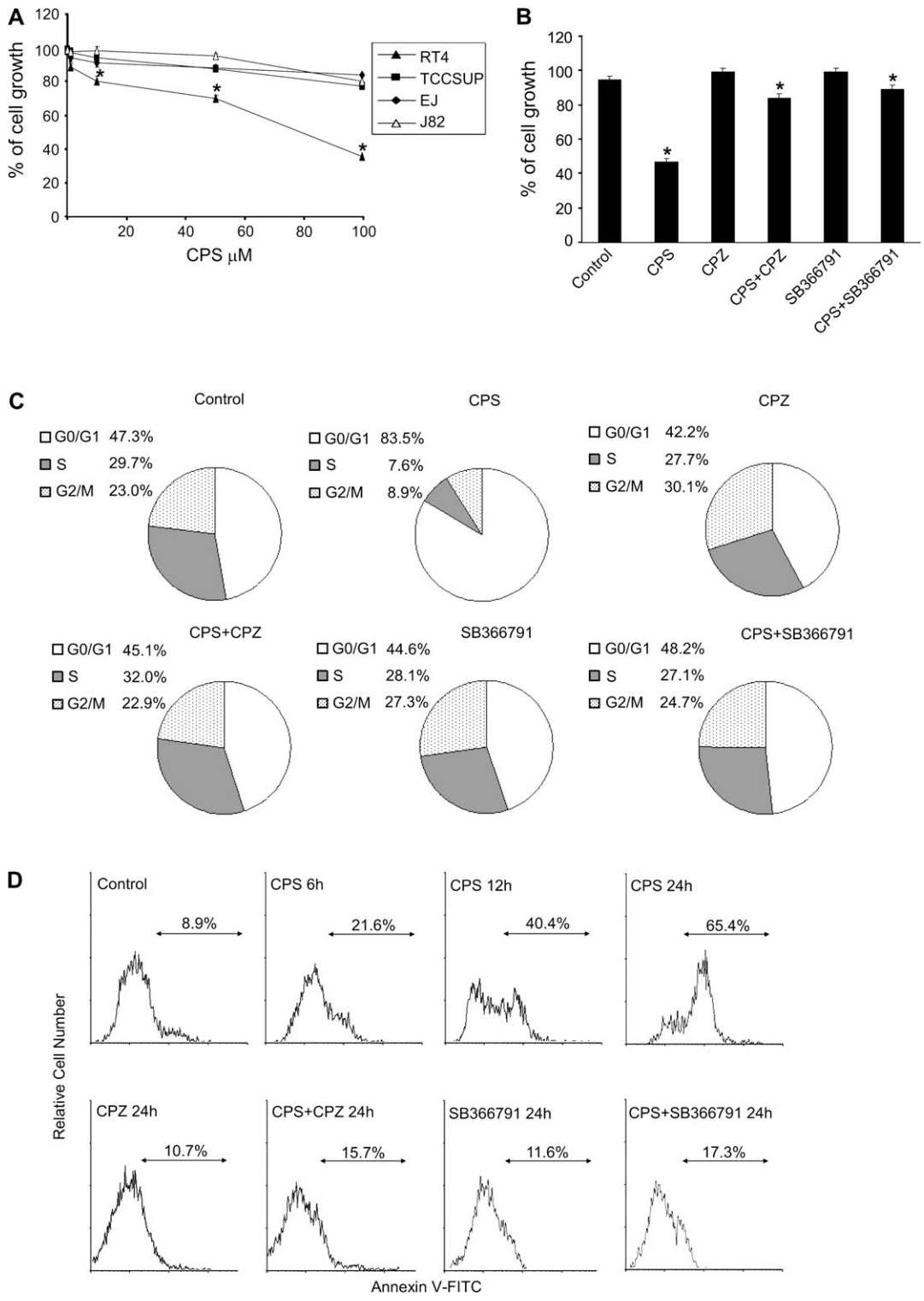

Fig. 2. CPS inhibits cell growth and induces G_0–G_1 cell growth arrest and apoptosis in RT4 cells. (**A**) Cell growth was evaluated by MTT assay in RT4, TCCSUP, J82 and EJ cell lines, untreated or treated for 24 h with different doses of CPS (10, 50 and 100 μM). Data are representative of three different experiments. Statistical analysis was performed comparing treated with untreated cells; $^{*}P < 0.01$. (**B**) Cell growth was evaluated by MTT assay in RT4 cells treated for 24 h with 100 μM CPS alone or in combination with CPZ (10 μM) or with SB366791 (0.1 μM). Control sample indicates dimethyl sulfoxide vehicle-treated cells. Statistical analysis was performed comparing CPS-, CPZ- or SB366791-treated RT4 cells with control and CPS plus CPZ- or CPS plus SB366791- with CPS-treated RT4 cells; $^{*}P < 0.01$. Data are representative of three different experiments. (**C**) Cell cycle analysis of RT4 cells treated with 100 μM CPS alone or in combination with CPZ (10 μM) or with SB366791 (0.1 μM) was performed by PI staining. Cell percentage relative to different cycle phases is indicated. Data are representative of three different experiments. (**D**) The percentage of AnnexinV^{+} RT4 cells treated at different times with 100 μM CPS alone or in combination with CPZ (10 μM) or with SB366791 (0.1 μM), was evaluated by immunofluorescence and FACS analysis. Control sample indicates dimethyl sulfoxide vehicle-treated cells. Data are representative of three different experiments.

significantly reduced in TCCSUP, J82 and EJ, cells as compared with NHUC (Figure 1A).

Analysis of TRPV1 protein expression by western blot revealed a doublet with apparent M_r of 97 and 114 kDa in particular in RT4 and NHUC (Figure 1B). No reactivity was observed with normal goat serum used as control (data not shown). Immunofluorescence and fluorescent activated cell sorting (FACS) analysis indicate that ~80% of RT4 cells express TRPV1, whereas negligible expression was observed in TCCSUP, J82 and EJ cells (Figure 1C). Confocal microscopy analysis evidenced TRPV1 in discrete spots in the plasma membrane and cytosol of RT4 cells (Figure 1D).

CPS arrests cell cycle progression and triggers apoptosis of RT4 cells

Several findings indicate that CPS inhibits cell growth *in vitro* and induces apoptosis in a TRPV1-dependent manner (1,3,4,17). We initially evaluated the effects of different doses (10 to 100 μM) of CPS on the growth of RT4, EJ, J82 and TCCSUP cells by MTT assay.

We found that CPS reduces in a dose-dependent manner (IC_{50} 80 μM) the growth of RT4 but not of the other UC cell lines examined (Figure 2A); this inhibition was completely reverted by CPZ or by SB366791, two specific TRPV1 antagonists (18,19) (Figure 2B). No cell death was observed with CPS, CPZ and SB366791 vehicles alone (data not shown).

Cell cycle analysis reveals that CPS increased the number of cells in G_0–G_1 and decreased those in S and G_2M phases, in a TRPV1-dependent manner, as evidenced by the ability of CPZ or of SB366791 to completely revert its effects (Figure 2C).

CPS-induced inhibition of RT4 cell growth was also associated with its pro-apoptotic activity, as shown by a time-dependent increase of annexin V binding (Figure 2D). This increase was mediated by TRPV1, as it was completely inhibited by CPZ or by SB366791. No increase in annexin V binding was observed in CPZ-treated or in SB366791-treated cells.

CPS-induced modulation of gene expression in RT4 cells

In an attempt to evaluate the molecular mechanisms underlying CPS pro-apoptotic effects, we performed a high-throughput mRNA expression profiling in RT4 cells at 4 and 12 h after CPS exposure, by using two different customized PCR arrays including genes involved in cell cycle control and DNA damage repair, signal transduction and transcription factors and apoptosis (Table I). Among the 168 defined genes examined, 5 genes were induced, 32 upregulated and 6 downregulated at 4 h after CPS treatment. In particular, among genes controlling cell cycle and DNA damage repair, *p53* and *E2F1* genes were induced and *ATM, WAF1/CIP1, CHK2, MDM2* and *GADD45A* were upregulated.

The intracellular transduction profiling of CPS-treated RT4 cells showed transient upregulation of ERBB2 and sustained upregulation of *MAP2K1* and *MYC* expression, whereas the transcriptional profiling revealed a transient increase of *NF-κB1* and a marked and sustained downregulation of *FOS* and *JUN* expression.

Moreover, the expression of genes classified as pro-apoptotic and anti-apoptotic of both intrinsic and extrinsic pathways were significantly modulated in CPS-treated RT4 cells. In particular, we observed upregulation of the pro-apoptotic Bcl-2 (*BAD, BCL10, BID* and *BAK1*), caspase (*caspases-8, -9, CFLAR* and *APAF1*) and death receptor (*Fas/CD95* and *TNFRSF10A* and *B, TNFRSF25, TRAF3* and *TRAF4*) families and induction of *BCLAF1* and *ABL-1*; expression of anti-apoptotic genes belonging to Bcl-2 family (*BCL2*, *BCL2L1*, *BAG3*, *BNIP2* and *MCL1*) and of the inhibitor of apoptosis protein (*IAP*) *BIRC2* was also increased. Finally, Bcl-2 interacting proteins, *BNIP3*, *BNIP3L* and *BIRC8*, were significantly downregulated. Interestingly, CPS also increased the expression of *RIPK2*, a serine/threonine kinase that associates Fas/CD95 and interacts with fas-associated protein with death domain and FLICE-inhibitory protein.

CPS induces TRPV1-Fas/CD95 receptor clustering and activation

Among the CPS-induced pro-apoptotic molecules, we focused our attention on Fas/CD95, a death receptor known to mediate apoptosis of UC cells (20).

We initially observed by immunofluorescence and FACS analysis that CPS-induced upregulation of Fas/CD95 mRNA in RT4 cells was accompanied by increased protein levels, at 12–24 h after CPS exposure (Figure 3A). Then, since Fas/CD95 ligand is not detectable on RT4 cells (data not shown), but ligand-independent Fas/CD95 clustering can also transmit apoptotic signal (21), we examined whether TRPV1 engagement by CPS could induce Fas/CD95 receptor clustering (Figure 3B). As shown by confocal microscopy, upon CPS treatment, TRPV1 and Fas/CD95 colocalized in a patched pattern indicating the translocation and co-clustering of both receptors. In contrast, a homogenous vesicular dispersed pattern was observed on the plasma membrane and cytoplasm of control cells (Figure 3C). CPS-induced Fas/CD95-TRPV1 co-clustering was TRPV1 dependent as it was abrogated by CPZ (Figure 3C).

Table I. Changes of gene expression induced by 100 μM CPS treatment in RT4 cells

Gene bank ID	Gene description	Fold change	
		4 h	12 h
NM_001160	APAF1	2.1[a]	—
NM_000051	ATM	2.5	—
NM_033341	BIRC8	−2.5	—
NM_004322	BAD	2.0	3.0
NM_004281	BAG3	2.8	—
NM_001188	BAK1	2.7	—
NM_003921	BCL10	3.7	—
NM_000633	BCL2	3.4	—
NM_138578	BCL2L1	IND[b]	
NM_014739	BCLAF1	IND	
NM_001196	BID	2.5	2.0
NM_001166	BIRC2	4.4	—
NM_004330	BNIP2	2.6	—
NM_004052	BNIP3	−7.0	−2.6
NM_004052	BNIP3L	−2.4	−2.3
NM_007294	BCRA1	2.5	—
NM_001228	Caspase-8	2.8	—
NM_001229	Caspase-9	3.1	—
NM_012114	Caspase-14	−29.9	−6.2
NM_003879	CFLAR	2.3	—
NM_007194	CHK2	2.2	—
NM_000389	WAF1/CIP1	2.9	—
NM_005225	E2F1	IND	
NM_000043	Fas/CD95	2.4	2.2
NM_006144	GZMA	5.5	6.4
NM_001924	GADD45A	2.6	—
NM_002392	MDM2	2.6	—
NM_002755	MAP2K1	2.7	2.0
NM_021960	MCL1	2.9	—
NM_003998	NF-κB1	2.0	—
NM_003821	RIPK2	3.4	2.0
NM_003862	TNFRSF10B	2.8	—
NM_001065	TNFRSF10A	2.0	—
NM_003790	TNFRSF25	2.8	2.0
NM_000546	P53	IND	
NM_005426	TP53BP2	4.2	—
NM_003300	TRAF3	2.6	—
NM_004295	TRAF4	3.0	—
NM_005157	ABLI	IND	
NM_004448	ERBB2	3.2	—
NM_005252	FOS	−2.3	−7.7
NM_002228	JUN	−2.6	−3.1
NM_002467	MYC	5.0	2.0

[a]Genes included are ≥2-fold upregulated or downregulated with respect to dimethyl sulfoxide vehicle RT4 cells used as control. Fold change >3 has a confidence interval of 99%, fold change >2 has a confidence interval of 90%. Mean of three biological repeats with similar general fold change is presented.

[b]IND: CPS-induced gene expression with respect to control cells.

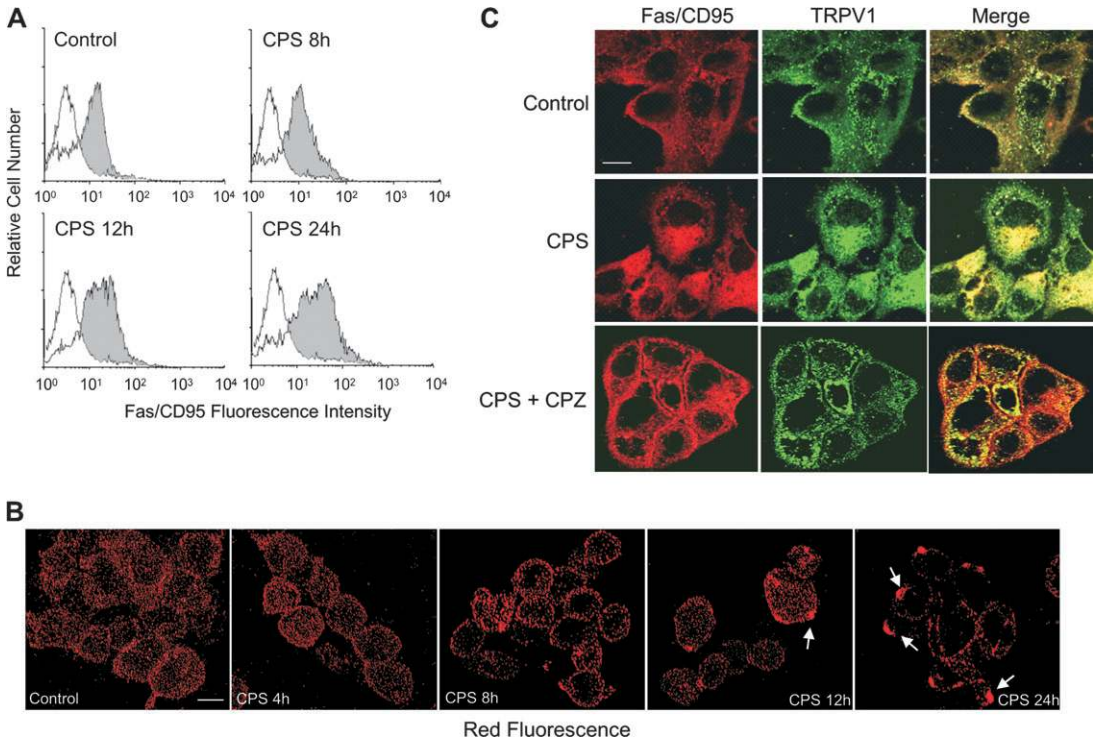

Fig. 3. CPS increases Fas/CD95 expression and clustering in TRPV1-dependent manner in RT4 cells. (**A**) Fas/CD95 expression was evaluated in RT4 cells treated for different times (8, 12 and 24 h) with 100 μM of CPS by immunofluorescence and FACS analysis using an anti-Fas/CD95 mAb followed by a phycoerythrin-conjugated GAM. Control sample indicates dimethyl sulfoxide vehicle-treated cells. White area indicates secondary Ab alone used as negative control. Data are representative of three different experiments. (**B**) Confocal laser scanning of Fas/CD95 clustering in RT4 cells treated for different times (4, 8, 12 and 24 h) with 100 μM of CPS. Control sample indicates dimethyl sulfoxide vehicle-treated cells. Data are representative of three different experiments. Arrows indicate Fas/CD95 clustering; bar = 10 μm. (**C**) The immunocytochemical localization of Fas/CD95 and TRPV1 in RT4 cells treated for 24 h with 100 μM of CPS alone or in combination with 10 μM of CPZ was analyzed by confocal microscopy using an anti-Fas/CD95 mAb and a goat anti-TRPV1 Ab followed by respective secondary Abs. Control sample indicates dimethyl sulfoxide vehicle. Data are representative of three different experiments; bar = 10 μm.

CPS triggers caspase-8 activation, BID cleavage, cytochrome c release, mitochondrial membrane potential ($\Delta\psi_m$) dissipation and caspases-9 and -3 activation in RT4 cells

Engagement of Fas/CD95 recruits fas-associated protein with death domain and pro-caspase-8 and then activated caspase-8 cleaves BID to generate an active p15 or truncated BID that translocates to the mitochondria where it produces the release of cytochrome c as a result of membrane permeability transition induction (22). Thus, we investigated whether CPS, despite increasing caspase-8, BID and caspase-9 mRNA (Table I), also resulted in their activation.

CPS induced caspase-8 activation at 8 h that increased at 12–24 h. In addition, we found that CPS treatment also stimulated BID cleavage, being the truncated BID expression first observed at 8 h, peaking at 12 h and was sustained at 24 h (Figure 4A).

We next determined whether CPS could induce cytochrome c release from mitochondria and whether membrane permeability transition induction was required for CPS-induced apoptosis. Eight hours after treatment, a band of 12 kDa corresponding to cytochrome c was observed and declined at later time points (Figure 4A). Evaluation of $\Delta\psi_m$ in RT4 cells by JC-1 labeling and FACS analysis showed that treatment with CPS induces a time-dependent decrease of red fluorescence and a concomitant increase of green fluorescence intensity (depolarization) (Figure 4B). CPS-induced $\Delta\psi_m$ dissipation was evident at 8 h, increased at 12 h and was maximal at 24 h.

Mitochondrion-dependent apoptosis is initiated by caspase-8 activation; thus, we evaluated the involvement of caspase-8 in CPS-induced $\Delta\psi_m$ dissipation by treating RT4 cells with the specific caspase-8 inhibitor, Z-IETD-FM, and we found a marked time-dependent inhibition of CPS-induced mitochondrial depolarization.

Finally, caspases-9 and -3 were activated during CPS-induced apoptosis of RT4 cells as shown by the appearance of their respective 34 and 17 kDa active fragments. Kinetic analysis indicates that caspase-9 activation precedes that of caspase-3, as caspase-9 is activated by CPS as early as 8 h and peaks at 12 h, whereas caspase-3 activation occurred at 12 h and persisted until 24 h after treatment (Figure 4D). No changes in caspase-3 activation were observed by treating RT4 cells with the caspase-8 inhibitor Z-IETD-FM (data not shown), thus suggesting that caspase-3 activation in CPS-treated RT4 cells is a caspase-9-dependent event.

CPS-induced ATM activation regulates p53 phosphorylation, Fas/CD95 expression and RT4 cell growth and apoptosis

Fas/CD95 expression is strictly regulated at transcriptional level by p53 whose activation and stabilization involves phosphorylation of multiple serine and threonine residues by a number of kinases including ATM, an atypical kinase initiating the DNA damage response through CHK2 activation (23). Thus, based on the transcriptional gene profiling showing increased expression of CHK2 and p53 mRNA, we investigated the role of ATM in CPS-induced p53 activation, Fas expression and clustering and apoptosis.

We initially examined the ability of CPS to trigger ATM activity in RT4 cells by evaluating the phosphorylation of serine 1981, an event functionally important for ATM activation. As shown by immunoblot, CPS stimulated ATM phosphorylation, which was evident at 1 h, peaked ~3 h and declined thereafter (Figure 5A). We then examined whether CPS could activate p53 in an ATM-dependent manner by using the specific pharmacological inhibitor KU55933. Analysis of p53 protein showed that its level rapidly increased at 1 h was maximal between 3 and 6 h and persisted until 24 h after CPS treatment (Figure 5A). Immunoblot analysis performed by using specific Abs against the Ser15, 20 and 392 phosphorylated p53 residues revealed that Ser15 becomes immediately (1–3 h) phosphorylated. Ser15

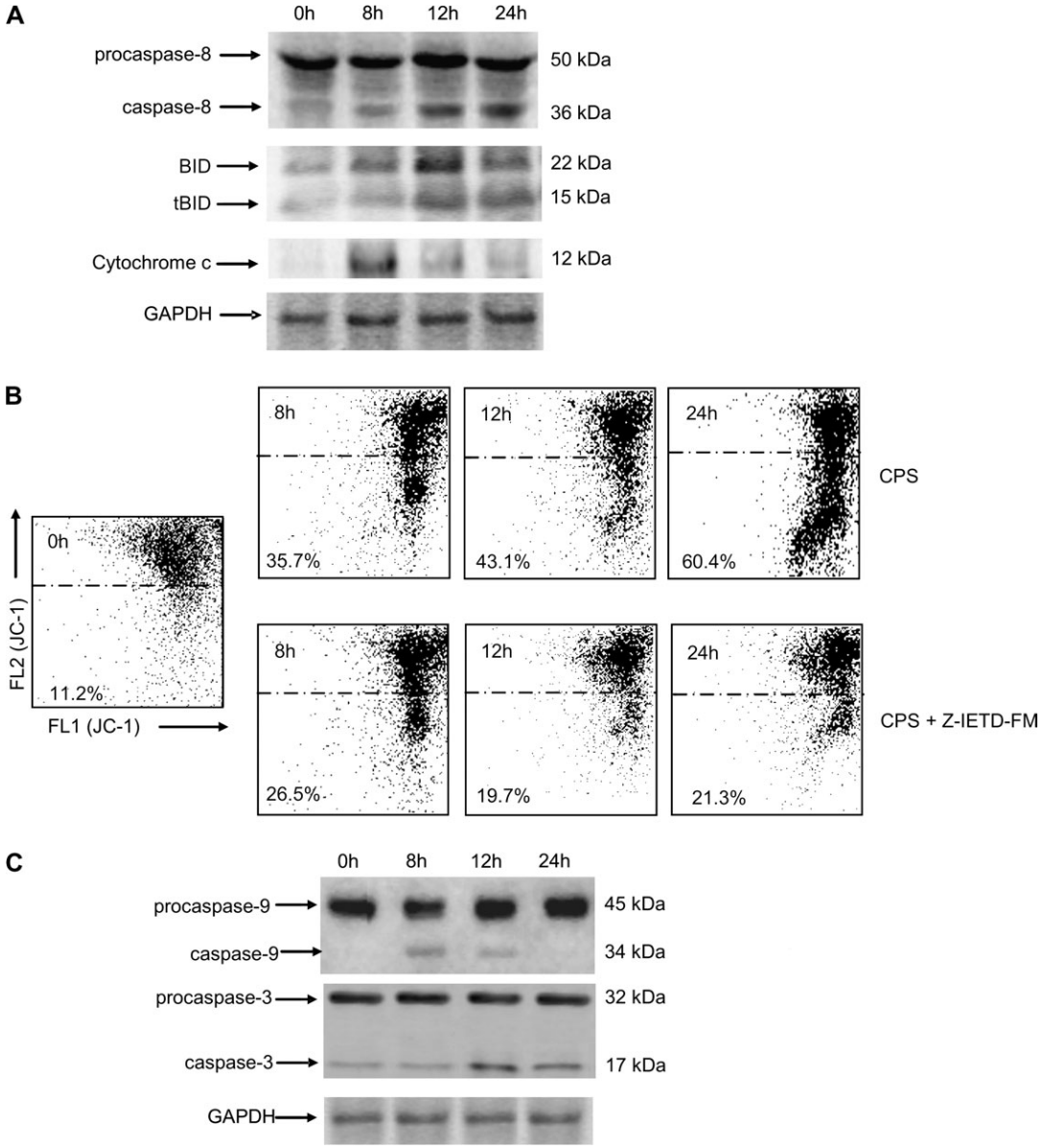

Fig. 4. CPS induces caspase-8 activation, BID cleavage, cytochrome c release, $\Delta\psi_m$ dissipation and caspase-9 and caspase-3 activation in RT4 cells. (**A**) Lysates from RT4 cells treated with 100 μM CPS at different times (8, 12 and 24 h) were separated on SDS–PAGE and probed with specific rabbit anti-caspase-8 Ab, rabbit anti-BID Ab or anti-cytochrome c mAb. Sizes are shown in kilodaltons (kDa) and arrows indicate the bands corresponding to procaspase-8, cleaved caspase-8 fragments, BID, truncated BID and cytochrome c. GAPDH levels were evaluated as protein loading control. Data are representative of three separate experiments. (**B**) Time course analysis of $\Delta\psi_m$ changes in RT4 cells treated for different times (8, 12 and 24 h) with 100 μM CPS alone or in combination with 50 μM Z-IED-FM was evaluated by JC-1 staining and biparametric FL1(green)/FL2(red) flow cytometric analysis. Numbers indicate the percentage of gated RT4 cells showing a drop in $\Delta\psi_m$-related red fluorescence intensity. Data are representative of three separate experiments. (**C**) Lysates from RT4 cells treated at different times (8, 12 and 24 h) with 100 μM CPS were separated on SDS–PAGE and probed with specific anti-caspase Abs. Sizes are shown in kilodaltons (kDa) and arrows indicate the bands corresponding to procaspase-9, cleaved caspase-9, procaspase-3 and cleaved caspase-3 fragment. GAPDH levels were evaluated as protein loading control. Data are representative of three separate experiments.

phosphorylation progressively declines at 6–12 h, returning to basal levels at 24 h after treatment; Ser20 is phosphorylated at later time points (3–6 h), and its phosphorylation remains sustained at 12–24 h whereas Ser392 phosphorylation occurs at 6–12 h and thereafter declines (Figure 5A).

Pretreatment of RT4 cells with KU55933 inhibited CPS-induced phosphorylation at both Ser15 and Ser20 whereas Ser392 sites (Figure 5B).

Inhibition of ATM activation by KU55933 also resulted in decreased induction of Fas/CD95 expression in CPS-treated RT4 cells as shown by immunofluorescence and FACS analysis (Figure 5C), as well as of Fas/CD95-TRPV1 co-clustering as assessed by confocal microscopy (Figure 5D). Moreover, KU55933 completely reverted CPS-mediated inhibition of RT4 cell growth (Figure 5E) and apoptosis (Figure 5F), as evaluated by MTT assay and annexin V staining and FACS analysis, respectively.

Discussion

A number of studies indicate the importance of the TRPV cation channels family in malignant cell growth and progression by controlling cell survival and apoptotic cell death (3,7,13,24,25).

Herein, we provide evidence on the expression of TRPV1 on human UC cell lines and its involvement in the apoptotic cell death

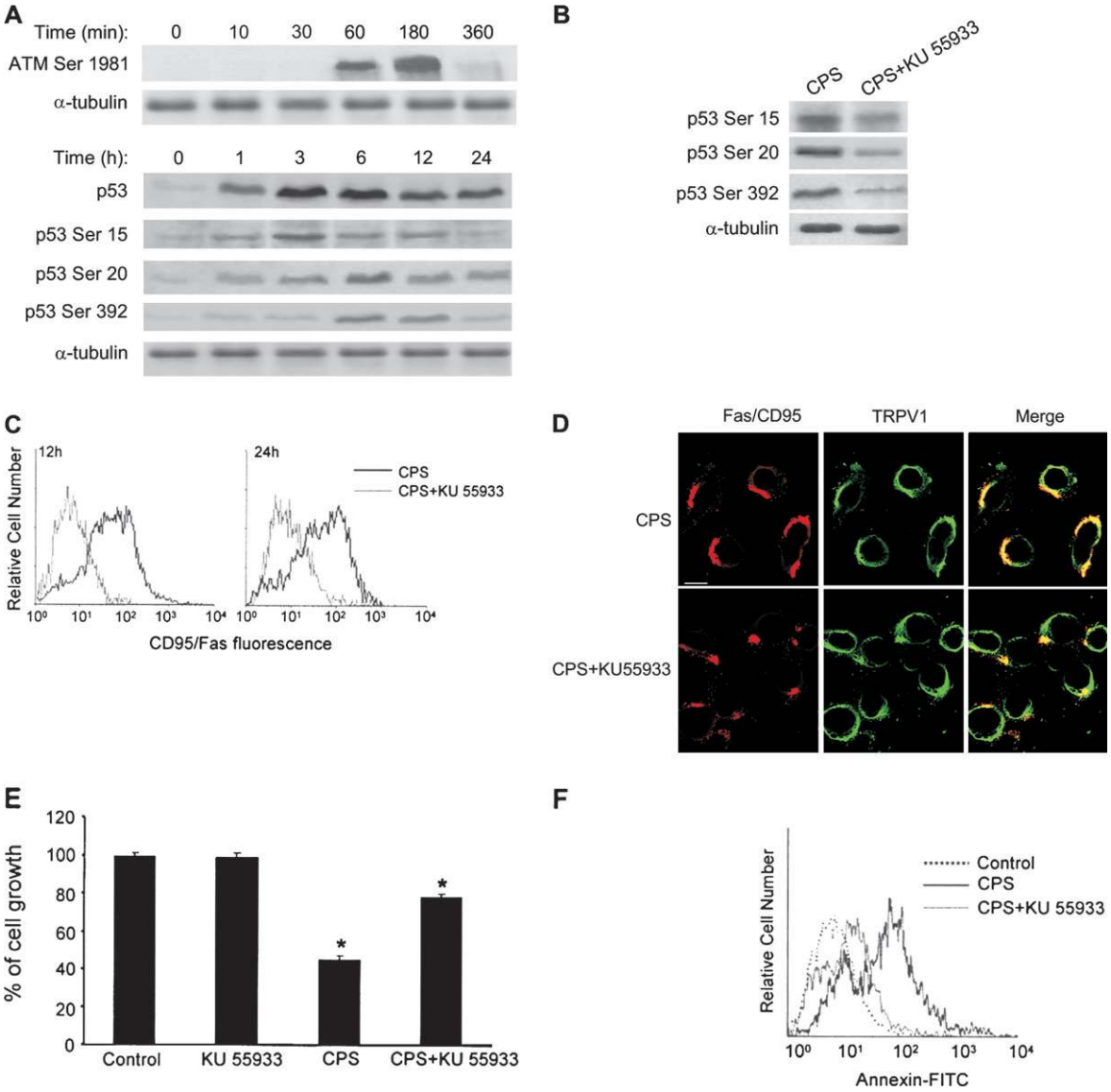

Fig. 5. CPS induces ATM activation that is involved in the control of p53 phosphorylation, Fas/CD95 expression and clustering and RT4 cell growth and apoptosis. (**A**) Lysates from RT4 cells treated at different times with 100 μM CPS were separated on 6 and 12% SDS–PAGE and probed with rabbit anti-phospho ATM (Ser1981) Ab or with a rabbit anti-human p53, phospho-p53 Ser15, phospho-p53 Ser20 or phospho-p53 Ser392 Abs, respectively. α-Tubulin levels were evaluated as protein loading control. Data are representative of three separate experiments. (**B**) Lysates from RT4 cells treated for 24 h with 100 μM CPS alone or in combination with 10 μM KU55933 were probed with rabbit anti-human phospho-p53 Ser15, Ser20 and Ser392 Abs. α-Tubulin levels were analyzed as protein loading control. Data are representative of three separate experiments. (**C**) Fas/CD95 expression was evaluated in RT4 cells treated for 12 and 24 h with 100 μM CPS alone or in combination with 10 μM KU55933, by immunofluorescence and FACS analysis using an anti-Fas/CD95 mAb followed by a phycoerythrin-conjugated GAM. Data are representative of three different experiments. (**D**) The immunocytochemical localization of Fas/CD95 and TRPV1 in RT4 cells treated for 24 h with 100 μM of CPS alone or in combination with 10 μM of KU55933 was evaluated as described in Figure 5 panel C; bar = 10 μm. (**E**) Cell growth was evaluated by MTT assay in RT4 cells treated for 24 h with 100 μM CPS and 10 μM KU55933 alone or in combination. Control sample indicates CPS and/or KU55933 vehicles treatment. Statistical analysis was performed comparing KU55933- or CPS-treated RT4 cells with control and CPS plus KU55933- with CPS-treated cells; $^{*}P < 0.01$. (**F**) Annexin-positive RT4 cells treated for 24 h with 100 μM CPS alone or in combination with 10 μM KU55933 was evaluated as described in Figure 3 panel D. Data are representative of three separate experiments.

induced by *in vitro* CPS treatment. In addition, our findings shed light on some of the molecular mechanisms regulating CPS-dependent TRPV1-mediated apoptosis, first underlying an important role for CPS-mediated ligand-independent Fas/CD95 clustering and activation of ATM/p53 pathway.

We found that TRPV1 mRNA and protein were expressed in well-differentiated RT4 papillary UC and NHUC cells, whereas they were markedly downregulated in poorly differentiated J82 and EJ and in undifferentiated TCCSUP UC cell lines. In RT4 cells, TRPV1 was identified as two bands of 114 and 97 kDa, probably corresponding to the glycosylated and non-glycosylated form of the receptor (26), and was distributed in discrete spots in the cytosol and plasma membrane; lower TRPV1 expression was found in TCCSUP, J82 and EJ cells.

The TRPV1-selective agonist CPS has been shown to inhibit the growth of various tumor cells *in vivo* and *in vitro* by inducing apoptosis (1). Our results first demonstrate the ability of CPS to induce G_0–G_1 cell cycle arrest and apoptosis in UC cells. CPS-mediated cell growth inhibitory effects are TRPV1 dependent and are completely reverted by the TRPV1 antagonists CPZ and SB366791. Similarly, induction of G_0–G_1 cell cycle arrest and apoptosis by CPS has been reported in human leukemic cells (2).

By high-throughput mRNA expression analysis, we demonstrate the ability of CPS to modulate a number of genes involved in cell cycle control, DNA damage repair and apoptosis. To more deeply investigate the molecular mechanisms underlying TRPV1-dependent CPS-induced apoptosis, we focused our attention on the death receptor Fas/CD95, on members of the caspase and Bcl-2 families and on ATM/CHK2/p53 DNA damage response pathway.

We show that CPS exposure significantly increases Fas/CD95 mRNA and protein expression and more importantly induces a TRPV1-dependent redistribution and clustering of Fas/CD95 that colocalizes with the vanilloid receptor. These findings suggest that Fas/CD95 ligand-independent TRPV1-mediated Fas/CD95 clustering results in death-inducing signaling complex formation and triggering of apoptotic signal. In accordance with our results, previous evidence demonstrates that TRPV1 N-terminus binds to fas-associated factor-1, a pro-apoptotic Fas/CD95-associated protein (27).

Consistent with TRPV1-mediated Fas/CD95 clustering, we show that CPS activates caspase-8 and BID cleavage and consequently the apoptotic extrinsic pathway. In addition, CPS augmented the expression of *caspase-8*, *CFLAR* and *RIPK2,* thus suggesting its role in the regulation of the extrinsic pathway also at transcriptional level.

In agreement with previous findings on other cell systems (1,5,17), we also show that CPS activates the mitochondrial intrinsic pathway of apoptotic cell death. In particular, we demonstrate that CPS causes cytochrome c release, $\Delta\psi_m$, dissipation and caspases-9 and -3 activation.

The CPS-induced $\Delta\psi_m$ dissipation was markedly inhibited by the specific caspase-8 inhibitor, Z-IETD-FM, thus suggesting a role of BID in cytochrome c release as shown previously (22). Moreover, we demonstrate that CPS treatment of RT4 cells increases procaspase-9 mRNA level and induces activation of caspases-9 and -3. The failure of the caspase-8 inhibitor, Z-IETD-FM to block CPS-induced activation of caspase-3, suggests that caspase-3 activation is a caspase-9-dependent event.

Fas/CD95 expression is strictly regulated at transcriptional level by p53 (27,28), whose activation and stabilization involve phosphorylation of multiple serine and threonine residues by a number of kinases including ATM (29).

Based on recent reports indicating that TRPV1 agonists cause ER stress and cell death (6,7) and that the ATM/CHK2/p53 pathway initiates the DNA damage response following ER-induced stress (30), we investigated the role of ATM in CPS-induced p53 activation, Fas/CD95 expression and clustering and RT4 cell apoptosis. Our results indicate that CPS by acting both at transcriptional and posttranscriptional levels induces a significant and time-dependent p53 protein accumulation and stabilization in RT4 cells. CPS treatment also stimulated p53 activation as shown by induced phosphorylation of Ser15, Ser20 and Ser392 residues, thus suggesting its involvement in CPS-induced upregulation of downstream *WAF1/CIP1*, *MDM2* and *GADD45A* gene expression. Time course of CPS-induced p53 phosphorylation suggests a site interdependence in p53 phosphorylation; thus, Ser15 was rapidly phosphorylated upon CPS treatment, followed by Ser20 and Ser392. In this regard, abrogation of Ser15 phosphorylation was found to prevent Ser20 phosphorylation (31), whereas phosphorylation of Ser392 was implicated in regulating p53 oligomerization and binding to DNA. Similarly to our results, CPS was reported to suppress the growth of leukemic cells via induction of G_0–G_1 phase cell cycle arrest, Ser15 p53 phosphorylation and apoptosis (2).

Our results provide also evidence that CPS treatment increases *ATM* and *CHK2* gene expression. In addition it rapidly stimulates Ser1981 ATM phosphorylation in RT4 cells and KU55933, a specific inhibitor of ATM kinase, completely blocks CPS-induced Ser15 and Ser20 and Ser392 p53 phosphorylation.

CPS-induced ATM activation correlates with the ability of this vanilloid to upregulate the expression of *E2F1* and *MYC* genes that can engage the DNA damage response, activate p53 and induce apoptosis (32). Of note, the use of KU55933 also revealed a role for ATM activation in the regulation of CPS-induced Fas/CD95 expression and co-clustering with TRPV1 and in the control of RT4 cell growth and apoptosis, thus suggesting an important link between ATM activation and Fas/CD95 apoptotic pathway.

Altogether, we describe a novel connection between ATM DNA damage response pathway and Fas/CD95 ligand-independent Fas/CD95-mediated intrinsic and extrinsic apoptotic pathways triggered by TRPV1 stimulation on UC cells.

The knowledge of the mechanisms controlling TRPV1 expression would be of importance for a better understanding of UC growth and progression. Moreover, as TRPV1 agonists such as CPS are widely employed in the treatment of lower urinary tract dysfunctions (33), the comprehension of the molecular mechanisms underlying their pro-apoptotic activity would be clinically relevant to extend the use of these agents also to the therapy of superficial urothelial malignancies.

Funding

AIRC Regional Grant (1116) and Ministero dell'Università e della Ricerca Scientifica e Tecnologica (MIUR), University of Camerino.

Acknowledgements

Conflict of Interest Statement: None declared.

References

1. Hail,N.Jr. (2003) Mechanisms of vanilloid-induced apoptosis. *Apoptosis*, **8**, 251–262.
2. Ito,K. *et al*. (2004) Induction of apoptosis in leukemic cells by homovanillic acid derivative, capsaicin, through oxidative stress: implication of phosphorylation of p53 at Ser-15 residue by reactive oxygen species. *Cancer Res.*, **64**, 1071–1078.
3. Amantini,C. *et al*. (2007) Capsaicin-induced apoptosis of glioma cells is mediated by TRPV1 vanilloid receptor and requires p38 MAPK activation. *J. Neurochem.*, **102**, 977–990.
4. Caterina,M.J. *et al*. (1997) The capsaicin receptor: a heat-activated ion channel in the pain pathway. *Nature*, **389**, 816–824.
5. Kim,S.R. *et al*. (2006) Transient receptor potential vanilloid subtype 1 mediates microgial cell death *in vivo* and *in vitro* via Ca2+-mediated mitochondrial damage and cytochrome c release. *J. Immunol.*, **177**, 4322–4329.
6. Thomas,K.C. *et al*. (2007) Transient receptor potential vanilloid 1 agonists cause endoplasmic reticulum stress and cell death in human lung cells. *J. Pharmacol. Exp. Ther.*, **321**, 830–838.
7. Sánchez,A.M. *et al*. (2008) Induction of the endoplasmic reticulum stress protein GADD153/CHOP by capsaicin in prostate PC-3 cells: a microarray study. *Biochem. Biophys. Res. Commun.*, **372**, 785–791.
8. Cortright,D.N. *et al*. (2004) Biochemical pharmacology of the vanilloid receptor TRPV1. An update. *Eur. J. Biochem.*, **271**, 1814–1819.
9. Avelino,A. *et al*. (2006) TRPV1 (vanilloid receptor) in the urinary tract: expression, function and clinical applications. *Naunyn Schmiedebergs Arch. Pharmacol.*, **373**, 287–299.
10. Birder,L.A. *et al*. (2001) Vanilloid receptor expression suggests a sensory role for urinary bladder epithelial cells. *Proc. Natl Acad. Sci. USA*, **98**, 13396–13401.
11. Birder,L.A. (2006) Urinary bladder urothelium: molecular sensor of chemical/thermal/mechanical stimuli. *Vascul. Pharmacol.*, **45**, 221–226.
12. Sanchez,M.G. *et al*. (2005) Expression of the transient receptor potential vanilloid 1 (TRPV1) in LNCaP and PC-3 prostate cancer cells and in human prostate tissue. *Eur. J. Pharmacol.*, **515**, 20–27.
13. Prevarskaya,N. *et al*. (2007) TRP channels in cancer. *Biochem. Biophys. Acta*, **1772**, 937–946.
14. Lazzeri,M. *et al*. (2005) Transient receptor potential vanilloid type 1 (TRPV1) expression changes from normal urothelium to transitional cell carcinoma of human bladder. *Eur. Urol.*, **48**, 691–698.
15. Maccarrone,M. *et al*. (2000) Anandamide induces apoptosis in human cells via vanilloid receptors. Evidence for a protective role of cannabinoid receptors. *J. Biol. Chem.*, **275**, 31938–31945.
16. Melck,D. *et al*. (2000) Suppression of nerve growth factor Trk receptors and prolactin receptors by endocannabinoids leads to inhibition of human breast and prostate cancer cell proliferation. *Endocrinology*, **141**, 118–126.
17. Amantini,C. *et al*. (2004) Distinct thymocyte subsets express the vanilloid receptor VR1 that mediates capsaicin-induced apoptotic cell death. *Cell Death Differ.*, **11**, 1342–1356.

18. Bevan,S. *et al*. (1992) Capsazepine: a competitive antagonist of the sensory neurone excitant capsaicin. *Br. J. Pharmacol.*, **107**, 544–552.
19. Gunthorpe,M.J. *et al*. (2004) Identification and characterisation of SB-366791, a potent and selective vanilloid receptor (VR1/TRPV1) antagonist. *Neuropharmacology*, **46**, 133–149.
20. Yamana,K. *et al*. (2005) Prognostic impact of FAS/CD95/APO-1 in urothelial cancers: decreased expression of Fas is associated with disease progression. *Br. J. Cancer*, **93**, 544–551.
21. Gajate,C. *et al*. (2000) Intracellular triggering of Fas, independently of FasL, as a new mechanism of antitumor ether lipid-induced apoptosis. *Int. J. Cancer*, **85**, 674–682.
22. Desagher,S. *et al*. (1999) BID-induced conformational change of Bax is responsible for mitochondrial cytochrome c release during apoptosis. *J. Cell Biol.*, **144**, 891–901.
23. Khanna,K.K. *et al*. (2001) ATM, a central controller of cellular responses to DNA damage. *Cell Death Differ.*, **8**, 1052–1065.
24. Fixemer,T. *et al*. (2003) Expression of the Ca2+-selective cation channel TRPV6 in human prostate cancer: a novel prognostic marker for tumor progression. *Oncogene*, **22**, 7858–7861.
25. Caprodossi,S. *et al*. (2008) Transient receptor potential vanilloid type 2 (TRPV2) expression in normal urothelium and in urothelial carcinoma of human bladder: correlation with the pathologic stage. *Eur. Urol.*, **54**, 612–620.
26. Kedey,N. *et al*. (2001) Analysis of the native quaternary structure of vanilloid receptor 1. *J. Biol. Chem.*, **276**, 28613–28619.
27. Kim,S. *et al*. (2006) TRPV1 recapitulates native capsaicin receptor in sensory neurons in association with Fas-associated factor 1. *J. Neurosci.*, **26**, 2403–2412.
28. Müller,M. *et al*. (1998) p53 activates the CD95 (APO-1/Fas) gene in response to DNA damage by anticancer drugs. *J. Exp. Med.*, **188**, 2033–2045.
29. Lavin,M.F. *et al*. (2006) The complexity of p53 stabilization and activation. *Cell Death Differ.*, **13**, 941–950.
30. Jinushi,M. *et al*. (2008) MHC class I chain-related protein A antibodies and shedding are associated with the progression of multiple myeloma. *Proc. Natl Acad. Sci. USA*, **105**, 1285–1290.
31. Saito,S. *et al*. (2003) Phosphorylation site interdependence of human p53 post-translational modifications in response to stress. *J. Biol. Chem.*, **278**, 37536–37544.
32. Hong,S. *et al*. (2006) Oncogene and the DNA damage response Myc and E2F1 engage the ATM signalling pathway to activate p53 and induce apoptosis. *Cell Cycle*, **8**, 801–803.
33. Birder,L.A. (2007) TRPs in bladder diseases. *Biochem. Biophys. Acta*, **772**, 879–884.

Received February 2, 2009; revised May 26, 2009; accepted May 28, 2009